Interventional MRI at High-Field (1.5 T): Needle Artifacts

Haiying Liu, PhD • Alastair J. Martin, PhD • Charles L. Truwit, MD

A better understanding of the appearance of a biopsy needle as well as its interaction with various sequence parameters in MRI is beneficial for its application in interventional MRI. As an extension of previous researchers' contributions, we investigate the specific characteristics of MR image artifacts associated with the tip of a biopsy needle when it is approximately parallel to the main magnetic field. The origin of the needle tip artifact, which exhibits as a blooming ball, was studied using MRI techniques and numerical simulation using the finite element method (FEM). Satisfactory agreement between theory and experiment has been achieved. Results showed that the image artifacts associated with biopsy needle are present and dependent on imaging parameters, but the artifacts can be reduced if optimal imaging parameters were used. Images of actual human brain tumor biopsies performed using the same needle under MRI guidance and monitoring demonstrated this artifact.

Index terms: Interventional MRI • Biopsy needles • Susceptibility artifact • Geometric image distortion • Device visualization

JMRI 1998; 8:214–219

Abbreviations: FE = field echo, FEM = finite element method, FLASH = fast low-angle shot, FOV = field of view, FSE = fast spin echo, LoLo = Local Look, RF = radiofrequency, SE = spin echo, TSE = turbo spin echo.

From the Center of Image Guided Therapy, Department of Radiology, University of Minnesota, 420 Delaware Street, SE, Minneapolis, Minnesota 55455. E-mail: liu@sparky.drad.umn.edu. Received July 3, 1997; revision requested August 15; revision received September 22; accepted October 21. **Address reprint requests to** H.L.

© ISMRM, 1998

THE INTEREST IN using MRI for guidance and monitoring of percutaneous interventions has been driven by MR's excellent soft tissue contrast, multiplanar capabilities and sensitivities to temperature, flow, susceptibility, etc. (1–5). The recent advances in MR and related technologies have resulted in a variety of cost-effective commercial "open MR" systems introduced for various investigation and clinical trials (5–7). In a continuous effort of exploring the potential of interventional MRI and as a complement to other interventional MRI groups, we have taken a venture at high field with a similar goal in the area of neurosurgery and neuroradiology.

The possibility of an induced magnetic force and an image artifact of a biopsy needle during interventional MRI have long been two primary concerns for the safety of MR image-guided surgical procedures and the quality of visualization and positional accuracy of the resulting images (1–3,5,9). Today, many of these obstacles have been overcome with the introduction of new materials with MR-friendly paramagnetic or diamagnetic properties, such as titanium alloy and carbon fiber composite. These materials have been critical to the development of a new generation of MR-compatible needles as well as other surgical instruments. Many careful studies have been conducted by various research groups to address these problems (8–13). Although metallic needles tend to have a more severe image artifact than that of carbon fiber, the metallic needles are often preferred because of clinical issues such as performance and visibility as well as practical issues such as machinability and cost. Today, interventional MRI is steadily pushing itself to more delicate neurologic surgical procedures in which much higher spatial precision is demanded. Therefore, any image artifact associated with the surgical instrument becomes an even more crucial problem. For interventional application at high field, the requirements for these MR-compatible devices (needles) are more stringent in terms of the need to control mechanical forces and imaging artifacts. Suitable materials for these needles as well as other surgical devices are generally the nonferromagnetic, inert, biocompatible, nontoxic materials such as titanium alloys, carbon fiber composite, copper, nonferromagnetic steel, etc. Disturbance of the uniform static magnetic field caused by a cylindrically shaped container filled with a solution of slightly different susceptibility from that of the surrounding can be predicted, and the resulting image distortion can be estimated (8). The image intensity artifacts and geometric distortion associated with a biopsy needle can be understood, to some extent, by mod-

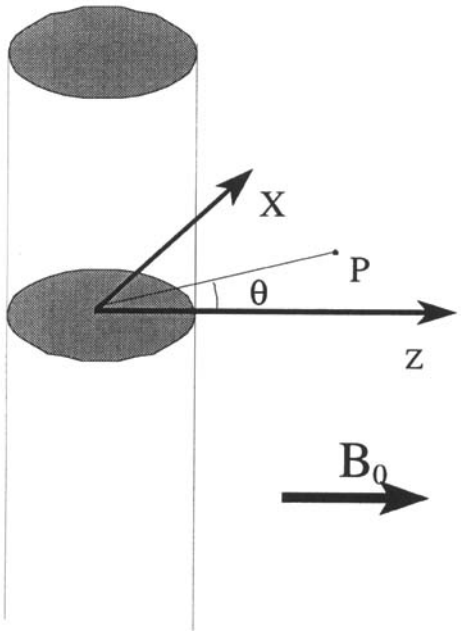

Figure 1. Schematic of a solid needle placed perpendicular to the direction of the main magnetic field denoted by B_0. The axis of the needle is assumed to be along the y axis.

eling a biopsy needle as an infinitely long solid cylinder in a uniform static magnetic field. A simple analytical expression can be obtained for the spatial dependence of the resulting external field perturbation, which clearly exhibits an orientational dependence. When a needle is positioned with its long axis perpendicular to the main magnetic field of the MRI scanner, as shown in Figure 1, the induced error field outside of the needle and far away from the two needle ends is given by the following (8,10):

$$\Delta\vec{B}_{out} = B_0\, a^2 \frac{\mu_n - \mu_t}{\mu_n + \mu_t}\left[\frac{z^2 - x^2}{(z^2 + x^2)^2}e_z + \frac{2zx}{(z^2 + x^2)^2}e_x\right] \quad [1]$$

where the long axis of the needle is assumed to be along the y axis, B_0 denotes the strength of the static uniform magnetic field (the direction of which is along the z direction as shown in Figure 1), μ_n and μ_t represent the magnetic permeability of the needle material and surrounding tissue, respectively, α is the radius of the needle, and e_x and e_z are two unit vectors denoting the directions of x and z axes. Inside the cylindrically shaped needle, the magnetic field error can be found analytically to be spatially uniform as given below.

$$\Delta\vec{B}_{in} = B_0 \frac{\mu_n - \mu_t}{\mu_n + \mu_t}e_z \quad [2]$$

The predictions of this analytical expression of the magnetic field have been validated by many groups and can be used as a basis for both simulation and correction of potential artifacts associated with various needles in interventional MRI. Both the positional and orientational dependence are clearly depicted in the expression. In the clinical setting, this theoretical background has limitations. For example, when a biopsy needle is placed parallel to the main static magnetic field (Fig. 2), the resulting image artifact is minimal along the length of the needle and exhibits a ball-shaped intensity void at its tip. The immediate concern is that the visualization of the tip location may be obscured by the image artifact. Without a clear understanding of its characteristics, this artifact inevitably poses a potential safety and accuracy problem

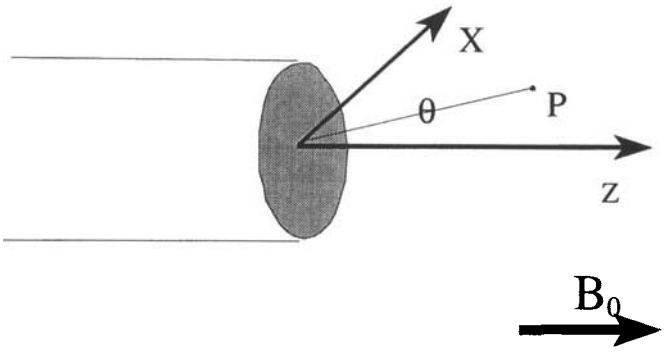

Figure 2. Schematic of a solid needle placed parallel to the direction of the main magnetic field denoted by B_0. The axis of the needle is assumed to be along the z axis. The shape of the tip is assumed to be flat.

in any clinical MR-guided procedure involving needles. The origin of this particular artifact has not been adequately described and understood. Clearly, this type of artifact cannot be well explained with the previous simplified model. In particular, the fact that a real needle is finite in length has not been fully considered in the model. In practice, cases involving small structures will require the artifact to be minimized and the true location of the needle tip with respect to the surrounding anatomy to be known with precision.

• MATERIALS AND METHODS

A nonferromagnetic titanium biopsy needle (Ruggles 2.5-mm diameter with a blunt tip, Elekta Instruments Inc., Atlanta, GA) has been used for both phantom studies and human brain tumor biopsies. In addition, another nonferromagnetic stainless steel needle was used in some imaging studies. All imaging experiments were conducted on a Philips 1.5-T whole-body MR scanner (ACS-NT, Best, Netherlands). A special phantom, which contained the needle immersed in water, has been constructed for studying the image artifact associated with a biopsy needle. As shown in Figure 3, this phantom incorporated a nonmagnetic grid structure for positional reference beneath the needle. For the purpose of understanding the image artifact, we have designed a set of comprehensive imaging and numerical studies. During MRI, the long axis of the needle was kept aligned with the direction of the main magnetic field (other orientations were also studied) and the tip of the needle was placed roughly at the isocenter of the magnet. For better signal-to-noise ratio, a receive-only head coil was used for the imaging experiments. The high resolution three-dimensional field-echo (FE) and spin-echo (SE) images at multiple data sampling bandwidths were obtained with a field of view (FOV) of 20 cm and data sampling matrix size of 256 × 256. To study the dependence on readout gradient direction, multiple directions were used for the readout gradient as well as two different polarities. Other relevant imaging techniques were used, such as two-dimensional (2D) SE and fast spin echo (FSE).

Numerical Simulation

According to the static magnetics theory, for zero external macroscopic current, a magnetic scalar potential as well as magnetic charge can be introduced. The surface magnetic charge density (σ) for a rounded needle tip as well as the bulk charge density (ρ) can be expressed as follows:

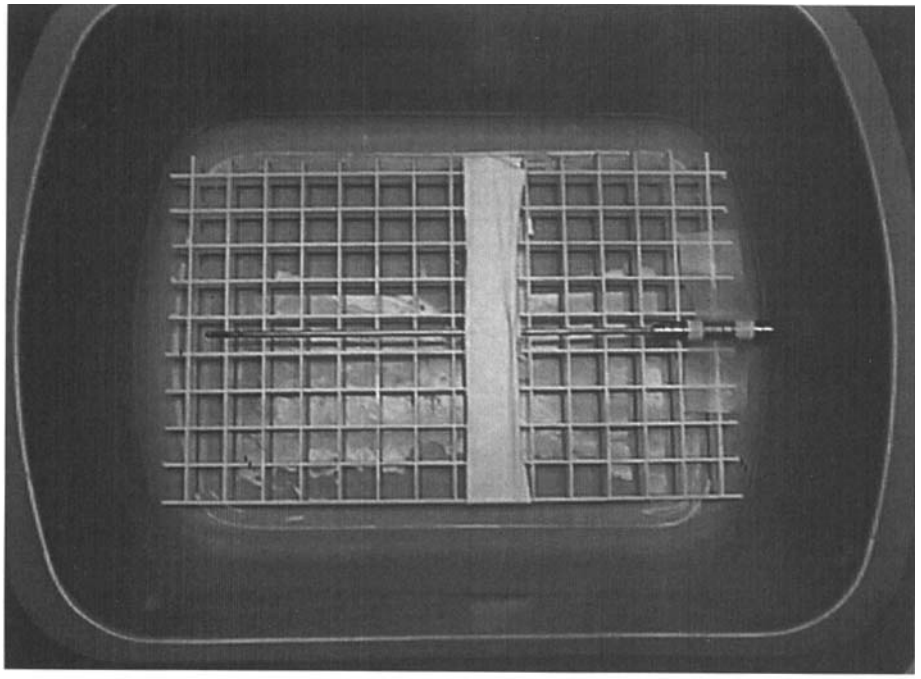

Figure 3. A close-up photo of the biopsy needle phantom showing a titanium needle with a blunt tip lying horizontally on a uniformly spaced plastic grid structure. The tip of needle was placed at the exact center of a square. The whole biopsy needle assembly consists of an outer sheath and an inner needle. The actual needle is hollow.

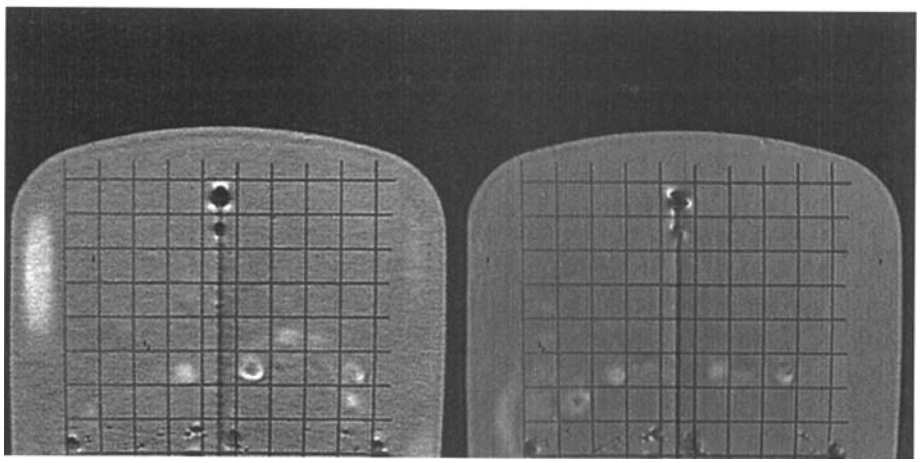

Figure 4. Two coronal three-dimensional FE images at the exact same slice position through the titanium needle with the readout gradient placed vertically (left) and horizontally (right). The main magnetic field direction is vertical. The size of the reference square is 15 × 15 mm. The needle tip was placed at the exact center of the square. Imaging parameters are: FOV = 20 cm, thickness = 4 mm, TR = 24 msec, TE = 3 msec, flip angle = 30°, image matrix size = 256 × 256, data sampling bandwidth = 81 Hz/pixel, number of signals averaged = 2.

$$\sigma_m = M_s \cdot n \qquad \rho_m = -\nabla \cdot M \qquad [3]$$

where M_s represents the magnetization M of the needle at the surface, and n denotes the surface unit normal vector of the spherical shaped tip. Because the magnetization of the needle-shaped object in a strong and uniform magnetic field is fairly uniform in the middle, there is no bulk charge density inside the needle away from the ends. The charge exists predominately on the surface and the ends. The bulk magnetization $M = \psi H$, where ψ is the magnetic susceptibility (for titanium [Ti], 1.8×10^{-4}; water, 8.8×10^{-6}) and H denotes the magnetic field intensity of the needle. At the end of the needle, because of the edge effect, H becomes spatially nonuniform because of the locally induced charges. The analytical solution for H is difficult to solve for; however, its numerical solution can be relatively easily obtained using a finite element method (FEM). By integrating the effect of the surface charge over both the surface area of the needle and the bulk charge over the volume of the needle, the total perturbation on the magnetic scalar potential in the vicinity of the tip of the needle can be obtained numerically for arbitrarily complex geometries.

$$\Phi(\vec{r}) = \frac{1}{4\pi}\int \frac{\sigma_m(\vec{r})}{|\vec{r}' - \vec{r}|}\,dS' + \frac{1}{4\pi}\int \frac{\rho_m(\vec{r}')}{|\vec{r} - \vec{r}'|}\,dV' \qquad [4]$$

where r denotes the coordinates for an observation point, r' denotes for the source coordinates. The perturbation on the magnetic flux density external to the needle can be obtained by taking the gradient of the resultant magnetic scalar potential.

$$\Delta\vec{B} = -\mu_0 \nabla\Phi \qquad [5]$$

An axisymmetric FEM model with a set of proper boundary conditions has been constructed for simulating the static magnetic behavior of a needle in a uniform magnetic field. From this model, using FEM solver software (ANSYS, Canonsburg, PA), we obtained the values for the internal and external H field from which the bulk magnetization was derived. From M, the charge densities can be determined. Integration of the field expression given above over the surface of the needle produced, as expected, the overall magnetic flux density disturbance that is localized at the tip of the needle. Starting from the resulting field perturbation of the static uniform main

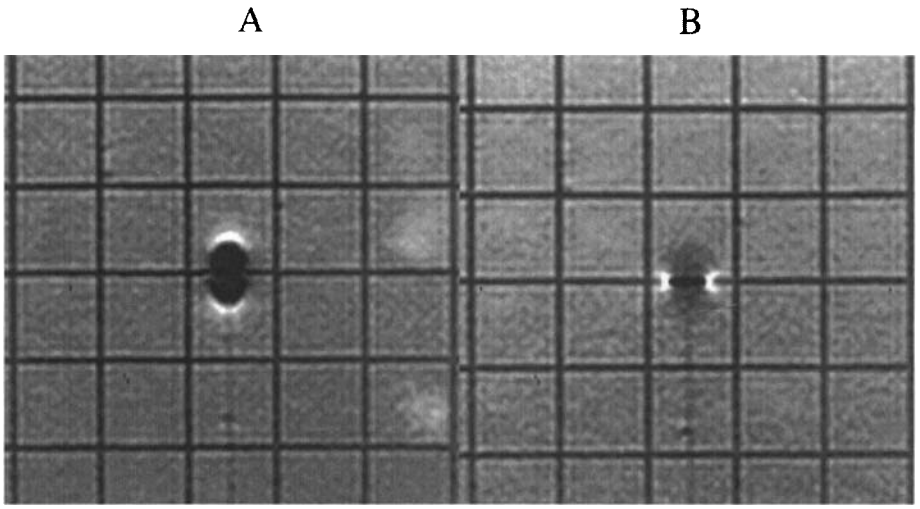

Figure 5. Two coronal two-dimensional SE images at the exact same slice position through a stainless steel needle with the readout gradient polarity vertically up **(a)** and vertically down **(b)**. The main static magnetic field direction is vertical. The size of the reference square is 15 × 15 mm. In this case, the tip of the needle was placed on the grid line. Imaging parameters are: FOV = 20 cm, thickness = 3 mm, TR = 500 msec, TE = 18 msec, matrix size = 256 × 256, data sampling bandwidth = 80 Hz/pixel.

magnetic field, various image artifacts, such as an image intensity void and an image geometric distortion, can be simulated and predicted for different imaging techniques. For the geometric image distortion, the deformed pixel location of image plane XY is characterized by the following coordinate mapping functions between the true (no superscript) and distorted (superscribed) values:

$$X^d = X + \frac{\delta B}{G_{rd}}$$
$$Y^d = Y \qquad [6]$$
$$Z^d = Z + \frac{\delta B}{G_{sl}}$$

where X and Y denote the readout axis and phase axis of an image plane, respectively, Z is the slice axis, δB is the field error along the direction of the main field, and G_{rd} and G_{sl} denotes the strength of the imaging readout gradient and slice-select gradient, respectively. For the image intensity, the intensity attenuation for a gradient-echo sequence is determined by a transverse inhomogeneity-induced intravoxel relaxation time constant denoted by τ, where

$$\tau \propto \nabla B \qquad [7]$$

Clinical Finding

In human applications, all brain tumor biopsies were performed under MR image guidance and monitoring in the newly established MR operating room, which has been carefully designed and tested for use in MR-guided neurosurgery. During biopsy, the patient's head was immobilized to the customized MR patient table by means of an MR-compatible head frame constructed of carbon fiber composite. After burr hole preparation on an operating table located directly in front of the magnet, the MR and operating room tables were docked and the patient was transferred to the MR scanner through this freely movable table. The biopsy procedure was performed at the rear end of the magnet, where MR images can be shown to the surgeon via an LCD panel. During the biopsy procedure, a fast MRI technique was selected based on its contrast (Local Look [LoLo] (14), T1 turbo spin echo [TSE], FLASH) and used interactively for needle trajectory guidance as well as positional verification. For the purpose of checking postprocedural complications, Flair, T2*, and T1 sequences were used.

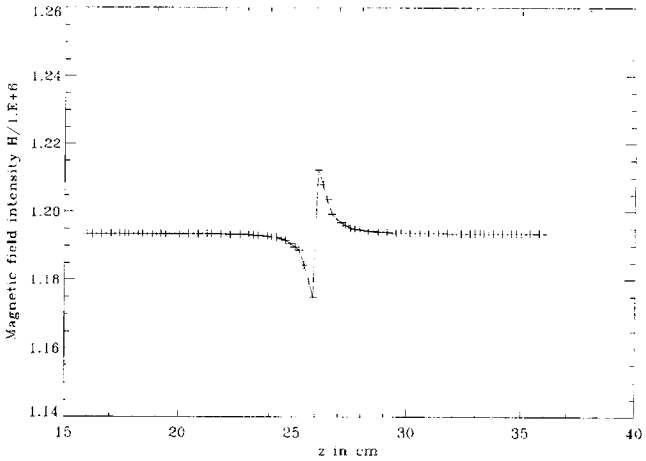

Figure 6. Magnetic field intensity (H) of the needle material along its axis at 1.5 T. Only one end of the needle is shown. The needle tip is at 10 cm, and the rest of the needle is on the left side of the 10-cm mark.

• RESULTS

When the needle and readout direction were placed parallel to the direction of the main magnetic field, a ball-shaped image artifact appeared on the resulting MR images of a three-dimensional field-echo acquisition as shown in Figures 4 and 5. Although the image artifact in the direction perpendicular to the needle becomes minimal along the middle of the needle stem, the size of the intensity void at the tip of the needle appears significantly larger than the diameter of the needle. The size of the artifact on this particular three-dimensional FE image is approximately 10 × 8.4 mm with the true location of the tip at the center of the artifact. The actual location of the needle tip was at the center of the reference square grid, the dimension of which was 15 × 15 mm. Generally, we found that the center of the artifact coincided with the true needle tip location. Furthermore, as the readout gradient is inverted, the appearance of the artifact is quite different (Fig. 5B). The resulting image artifact tends to collapse to a small perpendicular line at a level corresponding to the tip of the needle. As the readout gradient was tilted with respect to the needle, the resulting artifact shape followed the readout direction. For example, when the needle was placed at a 40° angle with respect to the z axis while keeping readout parallel to the main field, we

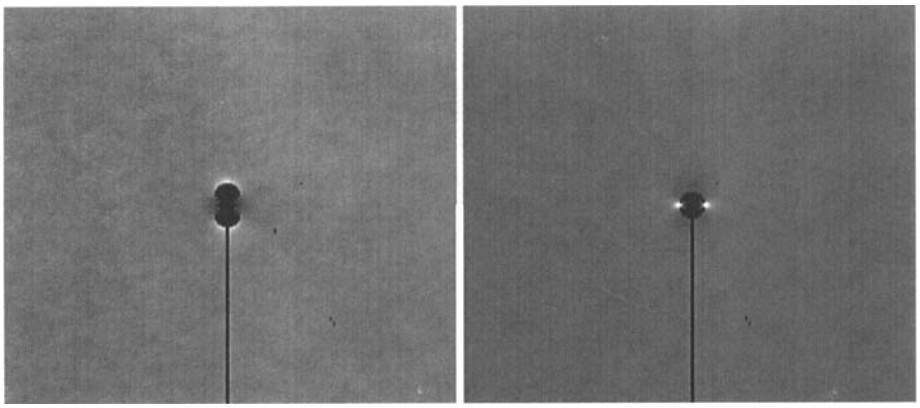

Figure 7. Two numerically simulated coronal two-dimensional SE images through the stainless steel needle with the read-out gradient polarity vertically up (left) and vertically down (right). The main magnetic field direction is vertical.

observed that the needle stem appeared wider as the angle increased. In addition, there still existed the same tip artifact along the readout direction. When the phase-encoding gradient was set to be perpendicular to the needle, the size of the artifact was reduced.

From a numerical simulation using a FEM solver, we obtained the needle magnetization and field patterns, one of which was the field intensity *H* inside the needle material as shown in Figure 6. Using the needle magnetization as an input, the field perturbation external to the needle was computed at high spatial resolution. Based on the calculated error field, an imaging experiment can be simulated if everything else is perfect. Simulated images reproduced the observed image artifact as shown in Figure 7.

• DISCUSSION

Figure 6 shows that the error magnetic field intensity (*H*) above and below the tip are pointing in opposite directions. This is consistent with the fact that the magnetic charge is mostly localized at the surface of the tip. At 1.5 T, based on a rough estimation assuming the needle is uniformly magnetized, the resulting field perturbation on the surface of the titanium needle tip can be as large as 5,760 Hz. This value drops quadratically as distance increases. In comparison, the typical bandwidth of radiofrequency (RF) pulses for many standard imaging applications is approximately 1,000 Hz. The consequence of this is an "off-resonance" image artifact. When the local Larmor frequency is altered beyond the RF excitation profile, the proton nuclear spins will not be excited at those locations, and thus, a signal void will be created on the resulting image. The shape of this type of intensity void will be determined by the error field contour line whose value in Hz equals the bandwidth of the RF pulse, and the size will be independent of the data sampling bandwidth. In other words, this artifact cannot be reduced by simply increasing the data sampling bandwidth. Besides, the ensemble magnetization dephasing depends on the local field inhomogeneity characterized by the local field gradient (the magnetic field suggests variation across an image pixel). Because the error magnetic field intensity (*H*) variation is abrupt at the tip, and so is the magnetic field (*B*) in the neighboring region external to the tip, one expects that there is substantial intravoxel dephasing in the local vicinity. This effect can always be reduced by using short TE and thereby minimizing dephasing time. On top of these two effects, there is the magnetic susceptibility induced geometrical image distortion, which can be described as a pixel shift along the readout direction on the resulting MR image. This positional shift is inversely proportional to the readout gradient strength or the data-sampling bandwidth. This image geometric distortion can be reduced by using a higher data-sampling bandwidth. The direction of the shift is also read gradient polarity dependent. Because the error magnetic field intensity (*H*) directions on two sides of the tip are opposite to each other, if the read gradient direction is parallel to the needle direction, the distortion shift directions for two sides are pointing away from each other and exhibit an artifact appearance similar to that shown in Figure 5A. If it is antiparallel, the shift on two sides are pointing toward each other and the artifact appearance is similar to that shown in Figure 5B. The predictions based on the numerical simulation for the imaging artifact shown in Figure 7 agreed qualitatively with the experimental results. Similar FEM simulations can be performed for more complex needles as well as tip structures at arbitrary orientation to obtain the detailed error field distribution.

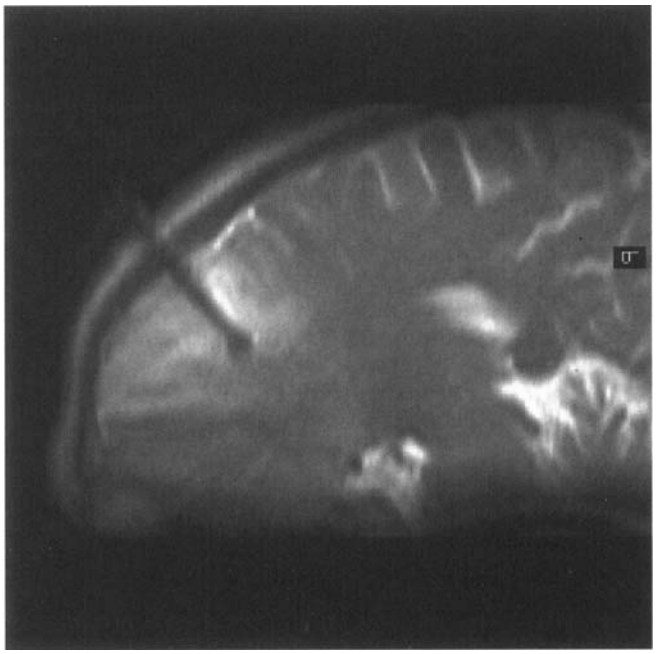

Figure 8. A 1-second LoLo T2-weighted image was acquired in an oblique sagittal plane during one of the brain tumor biopsies. The stem of the titanium needle appeared as an intensity void on the image. Note the artifact at the tip. The phase-encoding direction was vertical. Other imaging parameters are: FOV = 21 cm, with only 40% FOV in phase-encode direction; slice thickness = 7 mm; TR = 1,000 msec; TE = 45 msec; echo train length = 28; interecho spacing = 8.4 msec; 60% half Fourier acquisition; data sampling bandwidth = 224 Hz/pixel.

The readout gradient polarity plays a crucial role in determining the final shape of the artifact. To minimize the apparent artifact (distortion), the rule of thumb is to keep the readout gradient direction antiparallel to the direction the needle is pointing. This is completely general and applies to any needle orientation. This also ensures that the phase-encoding direction is always perpendicular to the needle (13). Furthermore, extra distortion at the vicinity of the tip alters both the appearance of the local anatomy as well as the shape of the needle. This, of course, invalidates positional reliability but may not be a problem for visualization because all of the anatomical structures, although deformed, are still there. A local geometrical distortion correction may be used to recover the true geometric representation through a warping technique. This will require incorporation of other needle-tracking schemes (15).

The same needle, which has passed a set of careful safety tests, has been used for various human brain biopsies under MR image guidance at 1.5 T. The corresponding MR images acquired during an actual brain tumor biopsy are shown in Figure 8, in which the needle stem was close to parallel to the direction of the main magnetic field. Notice the artifact intensity void at the tip of the needle.

In conclusion, we have shown the overall appearance of the MR image artifacts associated with the tip of a biopsy needle for various relevant imaging parameters and demonstrated that these image artifacts originate from both RF off-resonance effects and geometric distortion. A theoretical explanation has been introduced and validated using the MRI results. The same needle has been used routinely in real brain tumor biopsy procedures under MR monitoring yielding good results. Practical experience indicates that moderate image artifact to some extent enhances the visibility of the needle. Understanding the characteristics of the needle artifact and interaction with imaging parameters can help in not only optimizing the imaging parameter and technique to reduce the potential artifact but also in interpreting the artifact properly.

References

1. Mueller PR, Stark DD, Simeone JF, et al. MR-guided aspiration biopsy: needle design and clinical trials. Radiology 1986; 161: 605–609.
2. Lufkin RB, Teresi L, Hanafee WN. New needle for MR-guided aspiration cytology of the head and neck. Am J Roentgenol 1987; 149:380–382.
3. van Sonnenberg E, Hajek P, Gylys-Morin V, et al. A wire-sheath system for MR-guided biopsy and drainage: laboratory studies and experience in 10 patients. Am J Roentgenol 1988; 161:815–817.
4. Lufkin RB. Interventional MR imaging. Radiology 1995; 197: 16–18.
5. Silverman SG, Collick BD, Figueira MR, et al. Interventional MR-guided biopsy in an open-configuration MR imaging system. Radiology 1995; 197:175–181.
6. Schenck JF, Jolesz FA, Roemer PB, et al. Superconducting open configuration MRI system for image-guided therapy. Radiology 1995; 195:805–814.
7. De Salles AA, Lufkin RB. Minimally invasive therapy of the brain. New York: Thieme, 1997.
8. Ludeke KM, Roschmann P, Tischler R. Susceptibility artefacts in NMR imaging. Magn Reson Imaging 1985; 3:329–343.
9. Lewin JS, Duerk JL, Haaga JR. Needle localization in MR guided therapy: effect of field strength, sequence design, and magnetic field orientation. In: Proceedings of the 3rd annual scientific meeting of the Society of Magnetic Resonance. Nice: Society of Magnetic Resonance, 1995; 1155.
10. Ladd ME, Erhart P, Debatin JF, Romanoski BJ, Boesiger P, McKinnon GC. Biopsy needle susceptibility artifacts (abstract). Magn Reson Med 1996; 36:646–651.
11. Gehl HB, Frahm C, Melchert, Weiss HD. Suitability of different MR-compatible needle and magnet designs for MR-guided punctures. In: Proceedings of the 3rd annual scientific meeting of the Society of Magnetic Resonance. Nice: Society of Magnetic Resonance, 1995; 1156.
12. Lenz G, Dewey C. Study of new titanium alloy needles for interventional MRI procedures. In: Proceedings of the 3rd annual scientific meeting of the Society of Magnetic Resonance. Nice: Society of Magnetic Resonance, 1995; 1159.
13. Faber SC, Stehling MK, Reiser M. Artifacts of MR-compatible biopsy needles: optimization of pulse sequences, dependence on MR-parameters, comparison of different products. In: Proceedings of the 3rd annual scientific meeting of the Society of Magnetic Resonance. Nice: Society of Magnetic Resonance, 1995; 1741.
14. van Vaals JJ, van Yperen GH, Hoogenboom TLM, et al. Local Look (LoLo): zoom-fluoroscopy of a moving target. In: Proceedings of the 1st meeting of the Society of Magnetic Resonance. Dallas: Society of Magnetic Resonance, 1994; 38.
15. Dumoulin CL, Souza SP, Darrow RD. Real-time position monitoring of invasive device using magnetic resonance. Magn Reson Med 1993; 29:411–415.